MEDICAL RADIOLOGY

Diagnostic Imaging

M. F. Reiser · C. R. Becker · K. Nikolaou
G. Glazer (Eds.)

Multislice CT

3rd Revised Edition

With Contributions by

H. Alkadhi · G. Antoch · A. Ba-Ssalamah · A. Baur-Melnyk · C. R. Becker · C. Behrmann
T. A. Bley · D. Böckler · J. Boese · G. Brix · T. Brunner · A. Dirisamer · A. Dörfler
B. Ertl-Wagner · D. Fleischmann · T. Flohr · G. Glazer · A. Graser · J. Griebel
M. Hacker · P. Hallscheidt · C. Hassan · B. Heigl · C. J. Herold · C. P. Heußel
C. Hoeschen · M. H. K. Hoffmann · R.-T. Hoffmann · M. Hoheisel · F. Iafrate · L. Jäger
T. F. Jakobs · T. R. C. Johnson · W. A. Kalender · H.-U. Kauczor
K. Klingenbeck-Regn · C. Kölblinger · M. Körner · S. Kösling · A. Laghi · G. Lauritsch
A. Lembcke · J. Ley-Zaporozhan · U. Linsenmaier · J. Lutz · M. Macari · D. Maintz
O. Meissner · D. Morhard · U. G. Mueller-Lisse · C. Mueller-Mang · M. Nagel
E. A. Nekolla · K. Neumann · K. Nikolaou · M. Owsijewitsch · M. Pfister · C. Plank
G. Pöpperl · D. Regulla · M. F. Reiser · G. Richter · H. Ringl · P. Rogalla
E.-P. Rührnschopf · U. Saueressig · W. Schima · H. Schlattl · B. Scholz · B. Schreiber
H. Seifarth · B. Sommer · W. H. Sommer · M. Spahn · P. Stolzmann · N. Strobel
H. von Tengg-Kobligk · D. Theisen · C. G. Trumm · S. Ulzheimer · T. F. Weber
J.-E. Wildberger · M. Wintermark · B. J. Wintersperger · M. Zankl · C. J. Zech
M. Zellerhoff

Springer

Maximilian F. Reiser, MD, Professor
Christoph R. Becker, MD
Konstantin Nikolaou, MD
Institute of Clinical Radiology
Ludwig-Maximilians University
Munich University Hospital
Marchioninistrasse 15
81377 Munich
Germany

Gary Glazer, MD, Professor
Department of Radiology
Stanford University, School of Medicine
Room P-263
1201 Welch Road
Palo Alto, CA 94304
USA

Medical Radiology · Diagnostic Imaging and Radiation Oncology
Series Editors:
A.L. Baert · L.W. Brady · H.-P. Heilmann · M. Knauth · M. Molls · C. Nieder · K. Sartor

Continuation of Handbuch der medizinischen Radiologie
Encyclopedia of Medical Radiology

ISBN 978-3-540-33124-7 e-ISBN 978-3-540-33125-4

DOI 10.1007/978-3-540-33125-4

Library of Congress Control Number: 2008926739

Cover design: Verlagsservice Teichmann, Mauer, Germany
Production, reproduction and typesetting: le-tex publishing services oHG, Leipzig, Germany

Printed on acid-free paper

9 8 7 6 5 4 3 2 1

springer.com

Foreword

It is a great pleasure to introduce this third, completely revised and updated edition of the successful volume on multislice CT, which was first published in 2002.

It is amazing to observe the continuing rapid technological development in multislice CT and its new clinical applications. This volume again offers a comprehensive overview of all recent new experimental and clinical research in this field, but it also includes new chapters on dynamic volume CT with 320 detector rows and on flat detector CT. Numerous new and excellent illustrations help to push this book into an even higher scientific orbit.

I am again deeply indebted to the editors, M.F. Reiser, C.R. Becker, K. Nikolaou, and G. Glazer, for their high level of dedication and efforts to edit this 3rd volume in such a short time period in order to include all the latest advances in multislice CT. I also congratulate the editors and the contributing authors, all internationally well-known CT experts, on the in-depth coverage of the individual chapters.

This volume is a must for certified radiologists to update their knowledge and a source of basic information on CT for radiologists in training. Referring medical and surgical specialists will find it very useful for the daily clinical management of their patients.

Leuven

Albert L. Baert
Series Editor

Preface

Multi-detector row technology has become an established CT imaging modality worldwide. Nowadays, clinical applications such as multi-detector row CT angiography, and in particular cardiac CT, assume greater importance in daily routine. Furthermore, the scope of multi-detector row CT applications has expanded and requires different investigation strategies.

To exploit the full potential of multi-detector row CT, a fundamental knowledge of the technique and optimal investigation strategies in terms of patient preparation, contrast medium administration, and image interpretation is mandatory. The new generation of CT scanners, in particular dual-source CT, provides new opportunities and challenges by expanding the clinical applications.

The 5th International Symposium on Multi-Detector Row CT has brought together a variety of CT specialists with individual areas of expertise. This conference had a mission to educate the participants in multi-detector row CT skills rather than simply presenting the recent developments in technology and research. With about 1,000 attendees, this conference was a tremendous success and gained wide attention all over the world.

This volume has not been designed primarily as a reference book on multi-detector row CT. The idea of this book was rather to provide fundamental knowledge combined with an update on the latest CT scanner technology in challenging clinical areas. The book therefore supports the mission of the conference perfectly, with its profound discussion of different applications and investigation strategies.

We are grateful to Prof. Albert Baert for stimulating us to edit again this volume of the "Medical Radiology" series. The publisher, Springer-Verlag, enthusiastically supported the idea and provided us with invaluable assistance. We hope this book will be valuable to all those interested in multi-detector row CT.

Munich — Maximilian F. Reiser
Munich — Christoph R. Becker
Munich — Konstantin Nikolaou
Stanford — Gary Glazer

Contents

Technique

Neuro / Ear-Nose-Throat

Cardiovascular Imaging

Lung

Oncology

Intervention

Trauma Imaging / Acute Care

Technique

Multislice CT: Current Technology and Future Developments

1

Stefan Ulzheimer and Thomas Flohr

CONTENTS

S. Ulzheimer, PhD
Siemens Medical Solutions U.S.A., Inc., Computed Tomography Division, 51 Valley Stream Parkway, Malvern, PA, 19355, USA

T. Flohr, PhD
Siemens AG, Healthcare Sector, Business Unit Computed Tomography, Siemensstr. 1, 91301 Forchheim, Germany

ABSTRACT

Since its introduction in the early 1970s, computed tomography (CT) has undergone tremendous improvements in terms of technology, performance and clinical applications. Based on the historic evolution of CT and basic CT physics, this chapter describes the status quo of the technology and tries to anticipate future developments. Besides the description of key components of CT systems, a special focus is placed on breakthrough developments, such as multi-slice CT and dedicated scan modes for cardiac imaging.

1.1 Introduction

In 1972, the English engineer G.N. Hounsfield built the first commercial medical X-ray computed tomography (CT) scanner for the company EMI Ltd. as a pure head scanner with a conventional X-ray tube and a dual-row detector system moving incrementally around the patient. It was able to acquire 12 slices, each with a 13-mm slice thickness, and reconstruct the images with a matrix of 80×80 pixels (Fig. 1.1a) in approximately 35 min. Even though the performance of CT scanners increased dramatically over time until 1989, there were no principally new developments in conventional CT. By then, the acquisition time for one image decreased from 300 s in 1972 to 1–2 s, thin slices of down to 1 mm became possible, and the in-plane resolution increased from three line pairs per cm (lp/cm) to 10–15 lp/cm with typically 512 × 512 matrices.

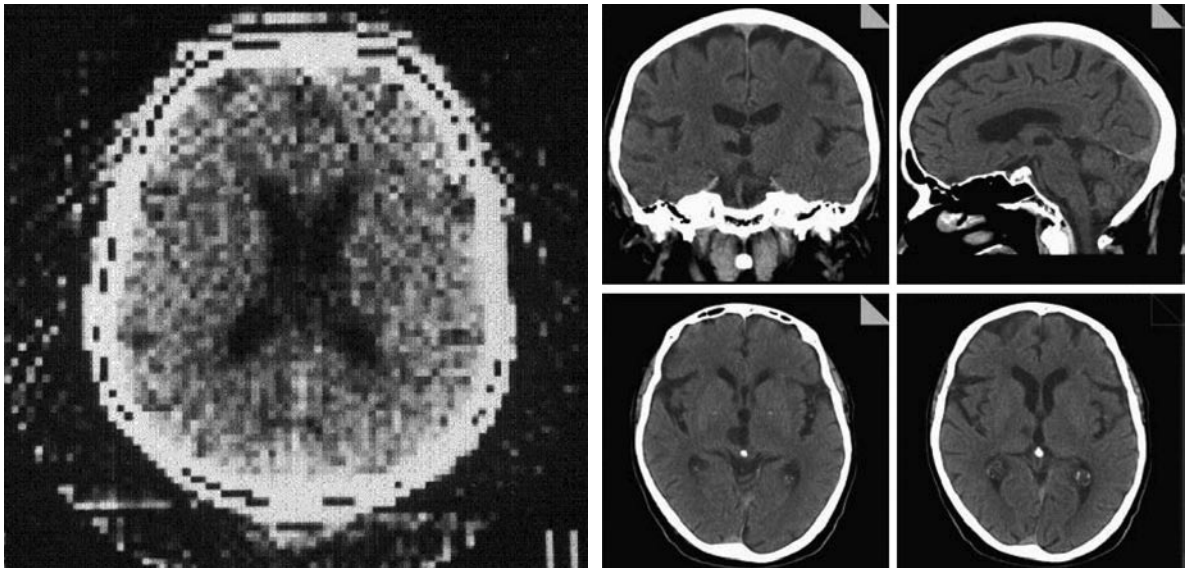

Fig. 1.1a,b. Development of computed tomography over time. **a** Cross-sectional image of a brain in the year 1971 and (**b**) the whole brain with sagittal, coronal and cross-sectional slices in the year 2007. (Image courtesy of Mayo Clinic Rochester)

As it was foreseen in the late 1970s that acquisition times of mechanical CT scanners would be far too long for high quality cardiac imaging for the next years or even decades to come, a completely new technical concept for a CT scanner without moving parts for extremely fast data acquisition of 50 ms was suggested and promoted as a cardiovascular CT (CVCT) scanner. Later, these scanners were also called "ultrafast CT" scanners or "electron beam CT" (EBT or EBCT) scanners. High cost and limited image quality combined with low volume coverage prevented the wide propagation of the modality, and the production and distribution of these scanners were discontinued.

Based on the introduction of slip ring technology to get power to and data off the rotating gantry, continuous rotation of the X-ray tube and the detector became possible. The ability of continuous rotation led to the development of spiral CT scanners in the early 1990s (Crawford and King 1990; Kalender et al. 1990), a method proposed already several years before (Mori 1986; Nishimura and Miyazaki 1988). Volume data could be acquired without the danger of mis- or double-registration of anatomical details. Images could be reconstructed at any position along the patient axis (longitudinal axis, *z*-axis), and overlapping image reconstruction could be used to improve longitudinal resolution. Volume data became the very basis for applications such as CT angiography (CTA) (Rubin et al. 1995), which has revolutionized non-invasive assessment of vascular disease. The ability to acquire volume data was the prerequisite for the development of three-dimensional image processing techniques such as multi-planar reformations (MPR), maximum intensity projections (MIP), surface shaded displays (SSD) or volume-rendering techniques (VRT), which have become a vital component of medical imaging today.

Main drawbacks of single-slice spiral CT are either insufficient volume coverage within one breath-hold time of the patient or missing spatial resolution in the *z*-axis due to wide collimation. With single-slice spiral CT, the ideal isotropic resolution, i.e., of equal resolution in all three spatial axes, can only be achieved for very limited scan ranges (Kalender 1995).

Larger volume coverage in shorter scan times and improved longitudinal resolution became feasible after the broad introduction of four-slice CT systems by all major CT manufacturers in 1998 (Klingenbeck-Regn et al. 1999; McCollough and Zink 1999; Hu et al. 2000). The increased performance allowed for the optimization of a variety of clinical protocols. Examination times for standard protocols could be significantly reduced; alternatively, scan ranges could be significantly extended. Furthermore, a given anatomic volume could be scanned within a given scan time with substantially reduced slice width. This way, for many clinical applications the goal of isotropic resolution was within reach with four-slice CT systems. Multi-detector row CT (MDCT) also dramatically expanded into areas previously considered beyond the scope of third-generation CT scanners based on the mechanical rotation of the

X-ray tube and detector, such as cardiac imaging with the addition of the ECG gating capability enabled by gantry rotation times down to 0.5 s (Kachelriess et al. 2000; Ohnesorge et al. 2000). Despite all these promising advances, clinical challenges and limitations remained for four-slice CT systems. True isotropic resolution for routine applications had not yet been achieved for many applications requiring extended scan ranges, since wider collimated slices (4×2.5 mm or 4×3.75 mm) had to be chosen to complete the scan within a reasonable timeframe. For ECG-gated coronary CTA, stents or severely calcified arteries constituted a diagnostic dilemma, mainly due to partial volume artifacts as a consequence of insufficient longitudinal resolution (Nieman et al. 2001), and reliable imaging of patients with higher heart rates was not possible due to limited temporal resolution.

As a next step, the introduction of an eight-slice CT system in 2000 enabled shorter scan times, but did not yet provide improved longitudinal resolution (thinnest collimation 8×1.25 mm). The latter was achieved with the introduction of 16-slice CT (Flohr et al. 2002a, 2002b), which made it possible to routinely acquire substantial anatomic volumes with isotropic sub-millimeter spatial resolution. ECG-gated cardiac scanning was enhanced by both improved temporal resolution achieved by gantry rotation time down to 0.375 s and improved spatial resolution (Nieman et al. 2002; Ropers et al. 2003).

The generation of 64-slice CT systems introduced in 2004 is currently the established standard in the high-end segment of the market. Two different scanner concepts were introduced by the different vendors: the "volume concept" was pursued by GE, while Philips and Toshiba aimed at a further increase in volume coverage speed by using 64 detector rows instead of 16 without changing the physical parameters of the scanner compared to the respective 16-slice version. The "resolution concept" pursued by Siemens uses 32 physical detector rows in combination with double *z*-sampling, a refined *z*-sampling technique enabled by a periodic motion of the focal spot in the *z*-direction, to simultaneously acquire 64 overlapping slices with the goal of pitch-independent increase of longitudinal resolution and reduction of spiral artifacts (Flohr et al. 2004, 2005a). With this scanner generation, CT angiographic examinations with sub-millimeter resolution in the pure arterial phase become feasible even for extended anatomical ranges. The improved temporal resolution due to gantry rotation times down to 0.33 s has the potential to increase clinical robustness of ECG-gated scanning at higher heart rates, thereby significantly reducing the number of patients requiring heart rate control and facilitating the successful integration of CT coronary angiography into routine clinical algorithms (Leschka et al. 2005; Raff et al. 2005). Today, high-end single-source scanners offer rotation times of down to 0.30 s and can acquire up to 128 slices with an isotropic resolution of down to 0.3 mm (Siemens SOMATOM Definition AS+). In late 2007, two manufacturers, Philips and Toshiba, introduced single-source scanners that can acquire 256 and 320 slices during one rotation, respectively, keeping "Moore's law of multi-slice CT (MSCT)" intact. When looking at the number of slices of multi-slice CT systems versus the year of their market introduction, the number of slices has increased exponentially as a function of time, roughly doubling every 2 years. This is an interesting parallel to Moore's law in the microelectronics sector. It remains to be seen how the recent enhancements in the number of slices translate into clinical benefits of these systems as only clinical performance will be able to justify the additional costs of such large detectors.

Pursuing a different path of technological advancement, in 2005, the first dual-source CT (DSCT) system, i.e., a CT system with two X-ray tubes and two corresponding detectors offset by 90°, was introduced by one vendor (Flohr et al. 2006). The key benefit of DSCT for cardiac scanning is the improved temporal resolution. A scanner of this type provides temporal resolution of a quarter of the gantry rotation time, independent of the patient's heart rate and without the need for multi-segment reconstruction techniques. DSCT scanners also show promising properties for general radiology applications. First, both X-ray tubes can be operated simultaneously in a standard spiral or sequential acquisition mode, in this way providing high power reserves when necessary. Additionally, both X-ray tubes can be operated at different kV settings and/or different pre-filtrations, in this way allowing dual-energy acquisitions. Potential applications of dual-energy CT include tissue characterization, calcium quantification and quantification of the local blood volume in contrast-enhanced scans.

1.2 System Design

The overall performance of a MDCT system depends on several key components. These components include the gantry, X-ray source, a high-powered generator, detector and detector electronics, data transmission systems (slip rings) and the computer system for image reconstruction and manipulation.

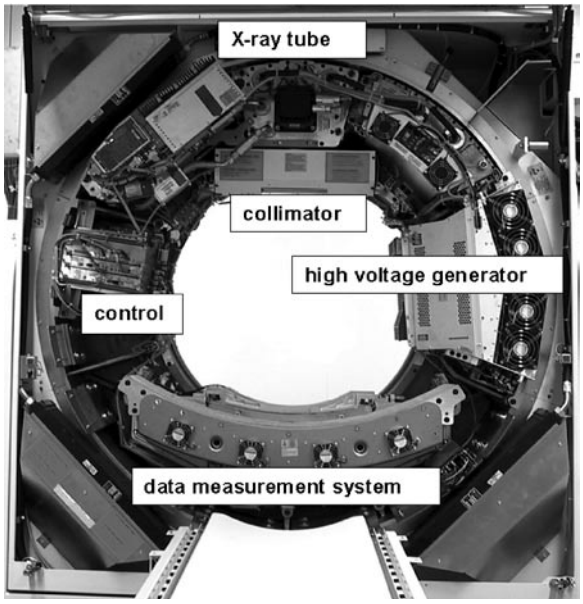

Fig. 1.2. Basic system components of a modern third-generation CT system. First-generation systems used a collimated pencil beam and therefore required a translation of the pencil beam and the single detector element before each rotational step to scan the whole object. Second-generation scanner used a small fan beam, but still required translational and rotational patterns of the X-ray source and the small detector array, whereas the fan beam of third-generation scanners the first time covered the whole object and allowed for a pure rotational motion of the tube and the detector around the patient

1.2.1 Gantry

Third-generation CT scanners employ the so-called "rotate/rotate" geometry, in which both the X-ray tube and detector are mounted onto a rotating gantry and rotate around the patient (Fig. 1.2). In a MDCT system, the detector comprises several rows of 700 and more detector elements that cover a scan field of view (SFOV) of usually 50 cm. The X-ray attenuation of the object is measured by the individual detector elements. All measurement values acquired at the same angular position of the measurement system form a "projection" or "view." Typically, 1,000 projections are measured during each 360° rotation. The key requirement for the mechanical design of the gantry is the stability of both focal spot and detector position during rotation, in particular with regard to the rapidly increasing rotational speeds of modern CT systems (from 0.75 s in 1994 to 0.30 s in 2007). Hence, the mechanical support for the X-ray tube, tube collimator and data measurement system (DMS) has to be designed so as to withstand the high gravitational forces associated with fast gantry rotation (~17 g for 0.42 s rotation time, ~33 g for 0.33-s rotation time).

1.2.2 X-Ray Tube and Generator

State-of-the-art X-ray tube/generator combinations provide a peak power of 60–100 kW, usually at various, user-selectable voltages, e.g., 80 kV, 100 kV, 120 kV and 140 kV. Different clinical applications require different X-ray spectra and hence different kV settings for optimum image quality and/or the best possible signal-to-noise ratio at the lowest dose. In a conventional tube design, an anode plate of typically 160–220-mm diameter rotates in a vacuum housing (Fig. 1.3). The heat storage capacity of anode plate and tube housing–measured in Mega Heat Units (MHU)–determines the performance level: the bigger the anode plate is, the larger the heat storage capacity, and the more scan-seconds can be delivered until the anode plate reaches its temperature limit. A state-of-the-art X-ray tube has a heat storage capacity of typically 5 to 9 MHU, realized by thick graphite layers attached to the backside of the anode plate. An alternative design is the rotating envelope tube (STRATON, Siemens, Forchheim, Germany, Schardt et al. 2004). The anode plate constitutes an outer wall of the rotating tube housing; it is therefore in direct contact with the cooling oil and can be efficiently cooled via thermal conduction (Fig. 1.3). This way, a very high heat dissipation rate of 5 MHU/min is achieved, eliminating the need for heat storage in the anode, which consequently has a heat storage capacity close to zero. Thanks to the fast anode cooling, rotating envelope tubes can perform high power scans in rapid succession. Due to the central rotating cathode, permanent electro-magnetic deflection of the electron beam is needed to position and shape the focal spot on the anode. The electro-magnetic deflection is also used for the double *z*-sampling technology of a 64-slice CT system (Flohr et al. 2004, 2005a).

1.2.3 MDCT Detector Design and Slice Collimation

Modern CT systems use solid state detectors in general. Each detector element consists of a radiation-sensitive solid-state material (such as cadmium tungstate, gadolinium-oxide or gadolinium oxi-sulfide with suitable dopings), which converts the absorbed X-rays into vis-

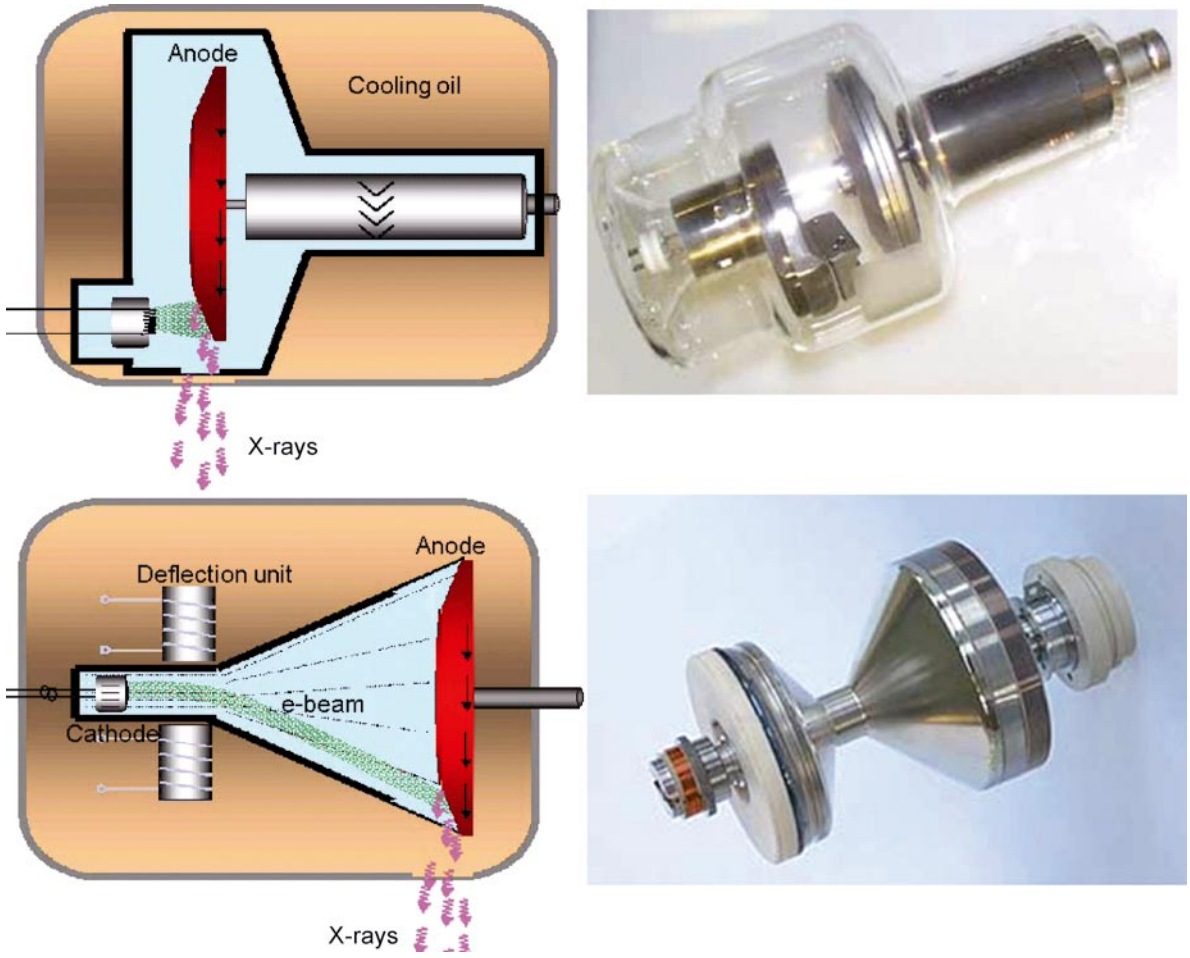

Fig. 1.3. Schematic drawings and pictures of a conventional X-ray tube (*top*) and a rotating envelope tube (*bottom*). The electrons emitted by the cathode are represented by *green lines*; the X-rays generated in the anode are depicted as *purple arrows*. In a conventional X-ray tube, the anode plate rotates in a vacuum housing. Heat is mainly dissipated via thermal radiation. In a rotating envelope tube, the anode plate constitutes an outer wall of the tube housing and is in direct contact with the cooling oil. Heat is more efficiently dissipated via thermal conduction, and the cooling rate is significantly increased. Rotating envelope tubes have no moving parts and no bearings in the vacuum. (Images not to scale)

ible light. The light is then detected by a Si photodiode. The resulting electrical current is amplified and converted into a digital signal. Key requirements for a suitable detector material are good detection efficiency, i.e., high atomic number, and very short afterglow time to enable the fast gantry rotation speeds that are essential for ECG-gated cardiac imaging.

CT detectors must provide different slice widths to adjust the optimum scan speed, longitudinal resolution and image noise for each application. With a single-slice CT detector, different collimated slice widths are obtained by pre-patient collimation of the X-ray beam. For a very elementary model of a two-slice CT detector consisting of M=2 detector rows, different slice widths can be obtained by pre-patient collimation if the detector is separated midway along the z-extent of the X-ray beam.

For M>2, this simple design principle must be replaced by more flexible concepts requiring more than M detector rows to simultaneously acquire M slices. Different manufacturers of MDCT scanners have introduced different detector designs. In order to be able to select different slice widths, all scanners combine several detector rows electronically to a smaller number of slices according to the selected beam collimation and the desired slice width.

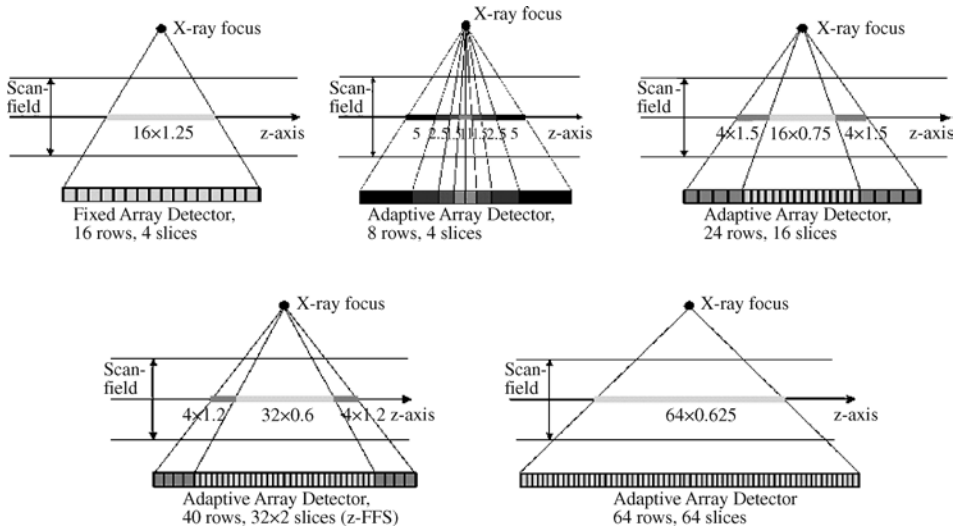

Fig. 1.4. Examples of fixed array detectors and adaptive array detectors used in commercially available MDCT systems

For the four-slice CT systems introduced in 1998, two detector types have been commonly used. The fixed array detector consists of detector elements with equal sizes in the longitudinal direction. A representative example for this scanner type, the GE Lightspeed scanner, has 16 detector rows, each of them defining 1.25-mm collimated slice width in the center of rotation (Hu et al. 2000; McCollough and Zink 1999). The total coverage in the longitudinal direction is 20 mm at iso-center; due to geometrical magnification, the actual detector is about twice as wide. In order to select different slice widths, several detector rows can be electronically combined to a smaller number of slices. The following slice widths (measured at iso-center) are realized: 4×1.25 mm, 4×2.5 mm, 4×3.75 mm and 4×5 mm (see Fig. 1.4, top left). The same detector design is used for the eight-slice version of this system, providing 8×1.25 mm and 8×2.5 mm collimated slice width.

A different approach uses an adaptive array detector design, which comprises detector rows with different sizes in the longitudinal direction. Scanners of this type, the Philips MX8000 four-slice scanner and the Siemens SOMATOM Sensation 4 scanner, have eight detector rows (Klingenbeck-Regn et al. 1999). Their widths in the longitudinal direction range from 1 to 5 mm (at iso-center) and allow for the following collimated slice widths: 2×0.5 mm, 4×1 mm, 4×2.5 mm, 4×5 mm, 2×8 mm and 2×10 mm (see Fig. 1.4, top center).

The 16-slice CT systems have adaptive array detectors in general. A representative example for this scanner type, the Siemens SOMATOM Sensation 16 scanner, uses 24 detector rows (Flohr et al. 2002a); see Fig. 1.4, top right. By appropriate combination of the signals of the individual detector rows, either 16 slices with 0.75-mm or 1.5-mm collimated slice width can be acquired simultaneously. The GE Lightspeed 16 scanner uses a similar design, which provides 16 slices with either 0.625-mm or 1.25-mm collimated slice width. Yet another design, which is implemented in the Toshiba Aquilion scanner, allows the use of 16 slices with 0.5-mm, 1-mm or 2-mm collimated slice width, with a total coverage of 32 mm at iso-center.

The Siemens SOMATOM Sensation 64 scanner has an adaptive array detector with 40 detector rows (Flohr et al. 2004). The 32 central rows define 0.6-mm collimated slice width at iso-center; the 4 outer rows on both sides define 1.2-mm collimated slice width (see Fig. 1.4, bottom left). The total coverage in the longitudinal direction is 28.8 mm. Using a periodic motion of the focal spot in the *z*-direction (*z*-flying focal spot), 64 overlapping 0.6-mm slices per rotation are acquired. Alternatively, 24 slices with 1.2-mm slice width can be obtained. Toshiba, Philips and GE use fixed array detectors for their 64-slice systems. The Toshiba Aquilion scanner has 64 detector rows with a collimated slice width of 0.5 mm. The total *z*-coverage at iso-center is 32 mm. Both the GE VCT scanner and the Philips Brilliance 64 have 64 detector rows with a collimated slice width of 0.625 mm, enabling the simultaneous read-out of 64 slices with a total coverage of 40 mm in the longitudinal direction (see Fig. 1.4, bottom right).

1.2.4 Data Rates and Data Transmission

With increasing numbers of detector rows and decreasing gantry rotation times, the data transmission systems of MDCT scanners must be capable of handling significant data rates: a four-slice CT system with 0.5-s rotation time roughly generates 1,000×700×4×2 bytes = 5.6 MB of data per rotation, corresponding to 11.2 MB/s; a 16-slice CT scanner with the same rotation time generates 45 MB/s, and a 64-slice CT-system can produce up to 180–200 MB/s. This stream of data is a challenge for data transmission off the gantry and for real-time data processing in the subsequent image reconstruction systems. In modern CT systems, contactless transmission technology is generally used for data transfer, which is either laser transmission or electro-magnetic transmission with a coupling between a rotating transmission ring antenna and a stationary receiving antenna. In the image reconstruction, computer images are reconstructed at a rate of up to 40 images/s for a 512×512 matrix using special array processors.

1.2.5 Dual-Source CT

A recently introduced dual-source CT (DSCT) system is equipped with two X-ray tubes and two corresponding detectors (Flohr et al. 2006). The two acquisition systems are mounted onto the rotating gantry with an angular offset of 90°. Figure 1.5 illustrates the principle. Using the *z*-flying focal spot technique (Flohr et al. 2004, 2005a), each detector acquires 64 overlapping 0.6-mm slices per rotation. The shortest gantry rotation time is 0.33 s. The key benefit of DSCT for cardiac scanning is improved temporal resolution. In a DSCT scanner, the half-scan sinogram in parallel geometry needed for ECG-controlled image reconstruction can be split up into two quarter-scan sinograms that are simultaneously acquired by the two acquisition systems in the same relative phase of the patient`s cardiac cycle and at the same anatomical level due to the 90° angle between both detectors. Details of cardiac reconstruction techniques can be found in Sect. 1.3.3 in this chapter.

With this approach, constant temporal resolution equivalent to a quarter of the gantry rotation time $t_{rot}/4$ is achieved in a centered region of the scan field of view. For t_{rot}= 0.33 s, the temporal resolution is $t_{rot}/4$ = 83 ms, independent of the patient's heart rate.

DSCT systems show interesting properties for general radiology applications, too. If both acquisition systems are simultaneously used in a standard spiral or sequential acquisition mode, up to 160 kW X-ray peak power is available. These power reserves are not only beneficial for the examination of morbidly obese patients, whose number is dramatically growing in western societies, but also to maintain adequate X-ray photon flux for standard protocols when high volume coverage speed is necessary. Additionally, both X-ray tubes can be operated at different kV and mA settings, allowing the acquisition of dual-energy data. While dual-energy CT was already evaluated 20 years ago (Kalender et al. 1986; Vetter et al.1986), technical limitations of the CT scanners at those times prevented the development of routine clinical applications. On the DSCT system, dual-energy data can be acquired nearly simultaneously

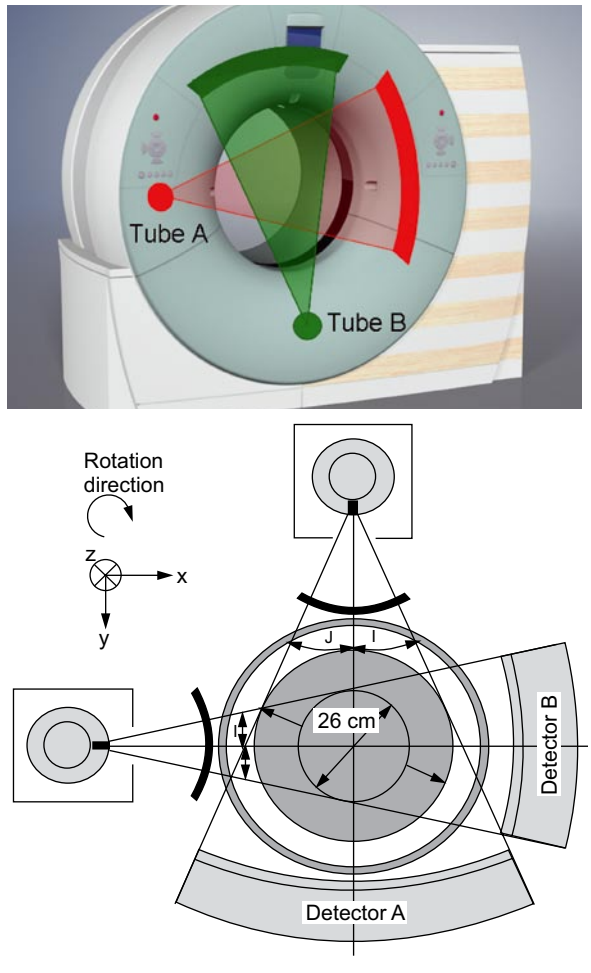

Fig. 1.5a,b. Schematic illustration of a dual-source CT (DSCT) system using two tubes and two corresponding detectors offset by 90°. A scanner of this type provides temporal resolution equivalent to a quarter of the gantry rotation time, independent of the patient`s heart rate. In a technical realization, one detector (**a**) covers the entire scan field of view with a diameter of 50 cm, while the other detector (**b**) is restricted to a smaller, central field of view

with sub-second scan times. The ability to overcome data registration problems should provide clinically relevant benefits. The use of dual-energy CT data can in principle add functional information to the morphological information based on X-ray attenuation coefficients that is usually obtained in a CT examination.
Figure 1.6 shows a clinical example to illustrate the clinical performance of DSCT for ECG-gated cardiac scanning.

1.3 Measurement Techniques

The two basic modes of MDCT data acquisition are axial and spiral (helical) scanning.

1.3.1 MDCT Sequential (Axial) Scanning

Using sequential (axial) scanning, the scan volume is covered by subsequent axial scans in a "step-and-shoot" technique. In between the individual axial scans, the table is moved to the next z-position. The number of images acquired during an axial scan corresponds to the number of active detector slices. By adding the detector signals of the active slices during image reconstruction, the number of images per scan can be further reduced, and the image slice width can be increased. A scan with 4×1-mm collimation as an example provides either four images with 1-mm section width, two images with 2-mm section width, or one image with 4-mm section width. The option to realize a wider section by summation of several thin sections is beneficial for examinations that require narrow collimation to avoid partial volume artifacts and low image noise to detect low contrast details, such as examinations of the posterior fossa of the skull or the cervical spine.

With the advent of MDCT, axial "step-and-shoot" scanning has remained in use for only few clinical applications, such as head scanning, high-resolution lung scanning, perfusion CT and interventional applications. A detailed theoretical description to predict the performance of MDCT in step-and-shoot mode has been given (Hsieh 2001).

1.3.2 MDCT Spiral (Helical) Scanning

Spiral/helical scanning is characterized by continuous gantry rotation and continuous data acquisition while the patient table is moving at constant speed; see Fig. 1.7.

1.3.2.1 Pitch

An important parameter to characterize a spiral/helical scan is the pitch p. According to IEC specifications (International Electrotechnical Commission 2002), p is given by:

p = table feed per rotation/total width of the collimated beam

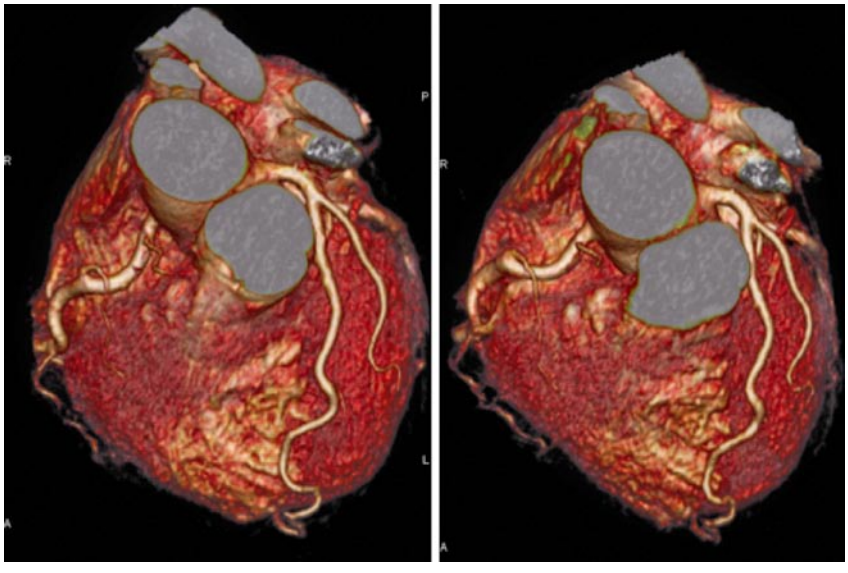

Fig. 1.6. Case study illustrating the clinical performance of dual-source CT (DSCT) for ECG-gated cardiac imaging. VRT renderings of a 59-year-old male patient with suspicion of RCA stenosis. The mean heart rate of the patient during the scan was 85 bpm. *Left*: Diastolic reconstruction at 65% of the cardiac cycle. *Right*: End systolic reconstruction at 28% of the cardiac cycle. In both cases the coronary arteries are clearly depicted with few or no motion artifacts

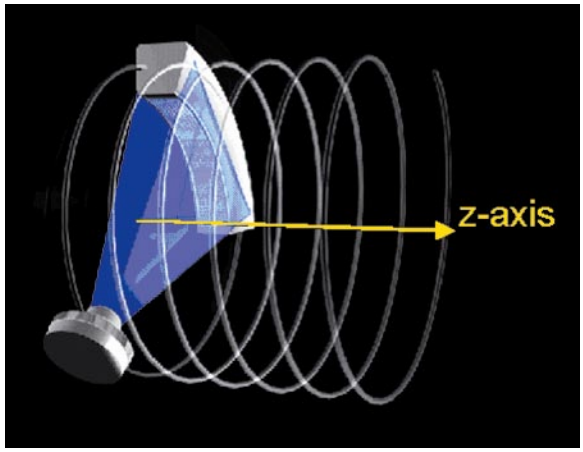

Fig. 1.7. Principle of spiral/helical CT scanning: the patient table is continuously translated while multiple rotations of scan data are acquired. The path of X-ray tube and detector relative to the patient is a helix. An interpolation of the acquired measurement data has to be performed in the *z*-direction to estimate a complete CT data set at the desired image position

This definition holds for single-slice CT as well as for MDCT. It shows whether data acquisition occurs with gaps ($p>1$) or with overlap ($p<1$) in the longitudinal direction. With 4×1-mm collimation and a table feed of 6 mm/rotation, the pitch is $p = 6/(4\times1) = 6/4 = 1.5$. With 16×0.75-mm collimation and a table feed of 18 mm/rotation, the pitch is $p = 18/(16\times0.75) = 18/12 = 1.5$, too. For general radiology applications, clinically useful pitch values range from 0.5 to 2. For the special case of ECG-gated cardiac scanning, very low pitch values of 0.2 to 0.4 are applied to ensure gapless volume coverage of the heart during each phase of the cardiac cycle.

1.3.2.2 Collimated and Effective Slice Width

Both single-slice and multi-slice spiral CT require an interpolation of the acquired measurement data in the longitudinal direction to estimate a complete CT data set at the desired plane of reconstruction. As a consequence of this interpolation, the slice profile changes from the trapezoidal, in some cases almost rectangular shape known from axial scanning to a more bell-shaped curve; see Fig. 1.8. The *z*-axis resolution is no longer determined by the collimated beam width S_{coll} alone (as in axial scanning), but by the effective slice width *s*, which is established in the spiral interpolation process. Usu-

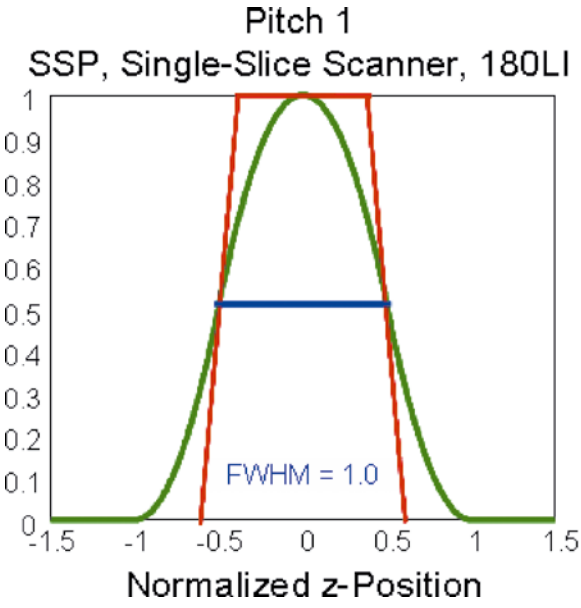

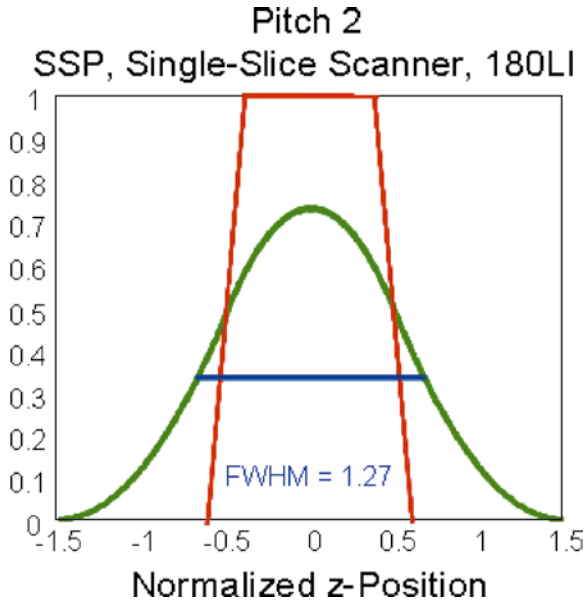

Fig. 1.8. Effective slice width in spiral/helical CT: the collimated slice profile, which is a trapezoidal in general, is indicated in *red*. The slice sensitivity profiles (*SSP*) after spiral/helical interpolation are bell-shaped; see the *green curves* for the most commonly used single-slice approach (180-LI) at different pitch values. 180-LI relies on a projection-wise linear interpolation of direct and complementary data. In spiral/helical CT, *z*-axis resolution is no longer determined by the collimated slice width alone, but by the effective slice width, which is defined as the Full Width at Half Maximum (*FWHM*) of the SSP

ally, S is defined as the Full Width at Half Maximum (FWHM) of the Slice Sensitivity Profile (SSP). The wider S_{coll} gets for a given collimated beam width S_{coll}, the more the longitudinal resolution degrades. In single-slice CT, S increases with increasing pitch (Fig. 1.9). This is a consequence of the increasing longitudinal distance of the projections used for spiral interpolation. The SSP is not only characterized by its FWHM, but by its entire shape: a SSP that has far-reaching tails degrades longitudinal resolution more than a well-defined, close to rectangular SSP, even if both have the same FWHM and hence the same effective slice width S. For a further characterization of spiral SSPs, the Full Width at Tenth Area (FWTA) is often considered in addition.

1.3.2.3 Multi-Slice Linear Interpolation and z-Filtering

Multi-slice linear interpolation is characterized by a projection-wise linear interpolation between two rays on either side of the image plane to establish a CT data set at the desired image z-position. The interpolation can be performed between the same detector slice at different projection angles (in different rotations) or different detector slices at the same projection angle. In general, scanners relying on this technique provide selected discrete pitch values to the user, such as 0.75 and 1.5 for four-slice scanning (Hu 1999) or 0.5625, 0.9375, 1.375 and 1.75 for 16-slice scanning (Hsieh 2003). The user has to be aware of the pitch-dependent effective slice widths S. For low-pitch scanning (at $p = 0.75$ using 4 slices and at $p = 0.5625$ or 0.9375 using 16 slices) $S \sim S_{coll}$ and for a collimated 1.25-mm slice the resulting effective slice width stays at 1.25 mm. The narrow SSP, however, is achieved by conjugate interpolation at the price of increased image noise (Hu et al. 1999; Hsieh 2003). For high-pitch scanning (at $p = 1.5$ using 4 slices and at $p = 1.375$ or 1.75 using 16 slices), $S \sim 1.27 S_{coll}$ and a collimated 1.25-mm slice results in an effective 1.5–1.6mm slice. To obtain the same image noise as in an axial scan with the same collimated slice width, 0.73–1.68 times the dose depending on the spiral pitch is required, with the lowest dose at the highest pitch (see Hsieh 2003). Thus, as a "take home point," when selecting the scan protocol for a particular application, scanning at low pitch optimizes image quality and longitudinal resolution at a given collimation, yet at the expense of increased patient dose. To reduce patient dose, either mA settings should be reduced at low pitch or high pitch values should be chosen.

In a z-filter multi-slice spiral reconstruction (Taguchi and Aradate 1998; Schaller et al. 2000), the spiral interpolation for each projection angle is no longer restricted to the two rays in closest proximity to the image

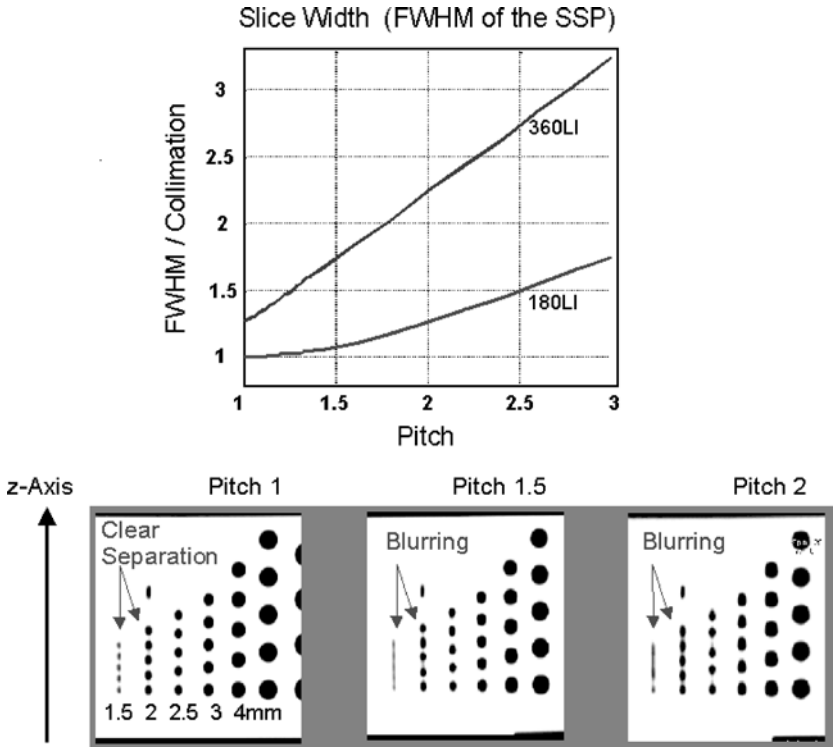

Fig. 1.9. *Top*: FWHM of the SSP as a function of the pitch for the two most commonly used single-slice spiral interpolation approaches, 180° linear interpolation (*180-LI*) and 360° linear interpolation (*360-LI*). For both, the slice significantly widens with increasing pitch as a result of the increasing distance of the interpolation partners. *Bottom*: MPRs of a spiral z-resolution phantom scanned with 2-mm collimation (180-LI) show increased blurring of the 1.5-mm and 2-mm cylinders with increasing pitch as a consequence of the increasing effective slice width

plane. Instead, all direct and complementary rays within a selectable distance from the image plane contribute to the image. A representative example for a *z*-filter approach is the Adaptive Axial Interpolation (Schaller et al. 2000) implemented in Siemens CT scanners. Another example is the MUSCOT algorithm (Taguchi and Aradate 1998) used by Toshiba. The *z*-filtering allows the system to trade off *z*-axis resolution with image noise (which directly correlates with required dose). From the same CT raw data, images with different slice widths can be retrospectively reconstructed. Only slice widths equal to or larger than the sub-beam collimation can be obtained. With the Adaptive Axial Interpolation the effective slice width is kept constant for all pitch values between 0.5 and 1.5 (Klingenbeck-Regn et al. 1999; Schaller et al. 2000; Fuchs et al. 2000). Therefore, longitudinal resolution is independent of the pitch; see Fig. 1.10. As a consequence of the pitch-independent spiral slice width, the image noise for fixed "effective" mAs (that is mAs divided by the pitch p) is nearly independent of the pitch. For 1.25-mm effective slice width reconstructed from 4×1-mm collimation, 0.61–0.69 times the dose is required to maintain the image noise of an axial scan at the same collimation (Fuchs et al. 2000). Radiation dose for fixed effective mAs is independent of the pitch and equals the dose of an axial scan at the same mAs. Thus, as a "take-home point," using higher pitch does not result in dose saving, which is an important practical consideration with CT systems relying on Adaptive Axial Interpolation and the "effective" mAs concept.

With regard to image quality, narrow collimation is preferable to wide collimation, due to better suppression of partial volume artifacts and a more rectangular SSP, even if the pitch has to be increased for equivalent volume coverage. Similar to single-slice spiral CT, narrow collimation scanning is the key to reduce artifacts and improve image quality. Best suppression of spiral artifacts is achieved by using both narrow collimation relative to the desired slice width and reducing the spiral pitch.

1.3.2.4 3D Back-Projection and Adaptive Multiple Plane Reconstruction AMPR

For CT scanners with 16 and more slices, modified reconstruction approaches accounting for the cone-beam geometry of the measurement rays have to be considered: the measurement rays in MDCT are tilted by the so-called cone angle with respect to a plane perpendicular to the *z*-axis. The cone angle is largest for the slices at the outer edges of the detector, and it increases with increasing number of detector rows if their width is kept

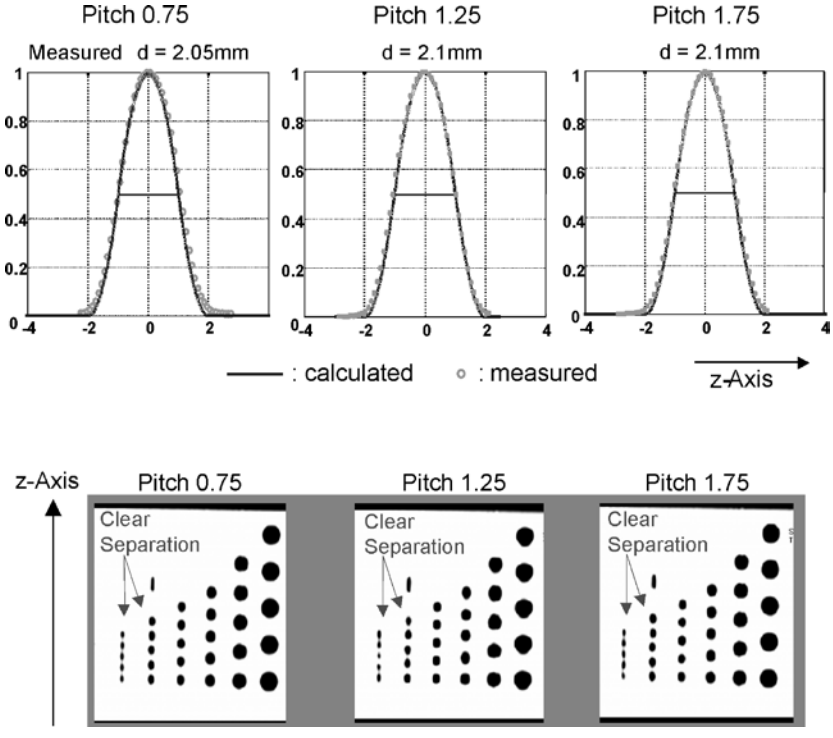

Fig. 1.10. Adaptive axial interpolation for a four-slice CT system: SSP of the 2-mm slice (for 4×1-mm collimation) at selected pitch values. The functional form of the SSP, and hence the effective slice width, are independent of the pitch. Consequently, MPRs of a spiral *z*-resolution phantom scanned with 2-mm slice width show clear separation of the 1.5-mm and 2-mm cylinders for all pitch values

constant. Some manufacturers (Toshiba, Philips) use a 3D filtered back-projection reconstruction (Feldkamp et al. 1984; Wang et al. 1993; Grass et al. 2000; Hein et al. 2003). With this approach, the measurement rays are back-projected into a 3D volume along the lines of measurement, this way accounting for their cone-beam geometry. Other manufacturers use algorithms that split the 3D reconstruction task into a series of conventional 2D reconstructions on tilted intermediate image planes. A representative example is the Adaptive Multiple Plane Reconstruction (AMPR) used by Siemens (Schaller et al. 2001a; Flohr et al. 2003a). Multi-slice spiral scanning using AMPR in combination with the "effective" mAs concept is characterized by the same key properties as Adaptive Axial Interpolation. Thus, all recommendations regarding selection of collimation and pitch that have been discussed there also apply to AMPR.

1.3.2.5 Double z-Sampling

The double *z*-sampling concept for multi-slice spiral scanning makes use of a periodic motion of the focal spot in the longitudinal direction to improve data sampling along the *z*-axis (Flohr et al. 2004, 2005a). By continuous electromagnetic deflection of the electron beam in a rotating envelope X-ray tube, the focal spot is wobbled between two different positions on the anode plate. The amplitude of the periodic *z*-motion is adjusted in a way that two subsequent readings are shifted by half a collimated slice width in the patient's longitudinal direction (Fig. 1.11). Therefore, the measurement rays of two subsequent readings with collimated slice width S_{coll} interleave in the *z*-direction, and every two *M*-slice readings are combined to one 2*M*-slice projection with a sampling distance of $S_{coll}/2$.

In the SOMATOM Sensation 64 (Siemens, Forchheim, Germany) as an example of a MDCT system relying on double *z*-sampling, two subsequent 32-slice readings are combined to one 64-slice projection with a sampling distance of 0.3 mm at the iso-center. As a consequence, spatial resolution in the logitudinal direction is increased, and objects <0.4 mm in diameter can be routinely resolved at any pitch; see Fig. 1.12. Another benefit of double *z*-sampling is the suppression of spiral "windmill" artifacts at any pitch (Fig. 1.13).

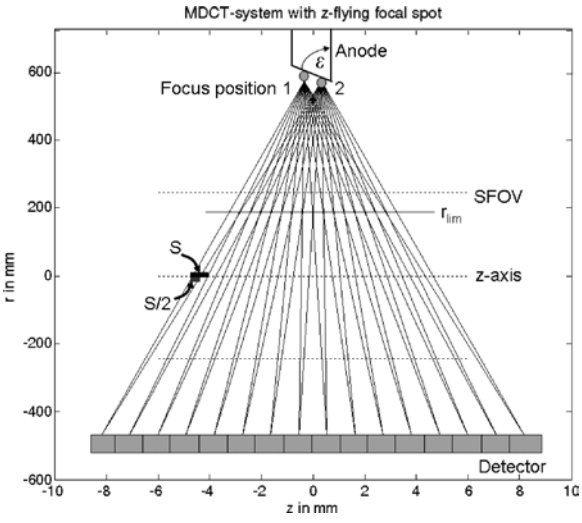

Fig. 1.11. Principle of improved *z*-sampling with the *z*-flying focal spot technique. Due to a periodic motion of the focal spot in the *z*-direction, two subsequent *M*-slice readings are shifted by half a collimated slice width S_{coll} /2 at iso-center and can be interleaved to one 2*M* slice projection

1.3.3 ECG-Triggered and ECG-Gated Cardio-Vascular CT

1.3.3.1 Principles of ECG Triggering and ECG Gating

For ECG-synchronized examinations of the cardiothoracic anatomy, either ECG-triggered axial scanning or ECG-gated spiral scanning can be used. A technical overview on ECG-controlled CT scanning can be found in Flohr et al. (2003b).

In ECG-triggered axial scanning, the heart volume is covered by subsequent axial scans in a "step-and-shoot" technique. The number of images per scan corresponds to the number of active detector slices. In between the individual axial scans, the table moves to the next *z*-position. Due to the time necessary for table motion, only every second heart beat can be used for data acquisition, which limits the minimum slice width to 2.5 mm with four-slice or 1.25 mm with eight-slice CT systems if the whole heart volume has to be covered within one breath-hold period. Scan data are acquired with a predefined temporal offset relative to the R-waves of the patient's ECG signal, which can be either relative (given as a certain percentage of the RR-interval time) or absolute (given in ms) and either forward or reverse (Ohnesorge et al. 2000; Flohr and Ohnesorge 2001); see Fig. 1.14.

To improve temporal resolution, modified reconstruction approaches for partial scan data have been proposed (Ohnesorge et al. 2000; Flohr and Ohne-

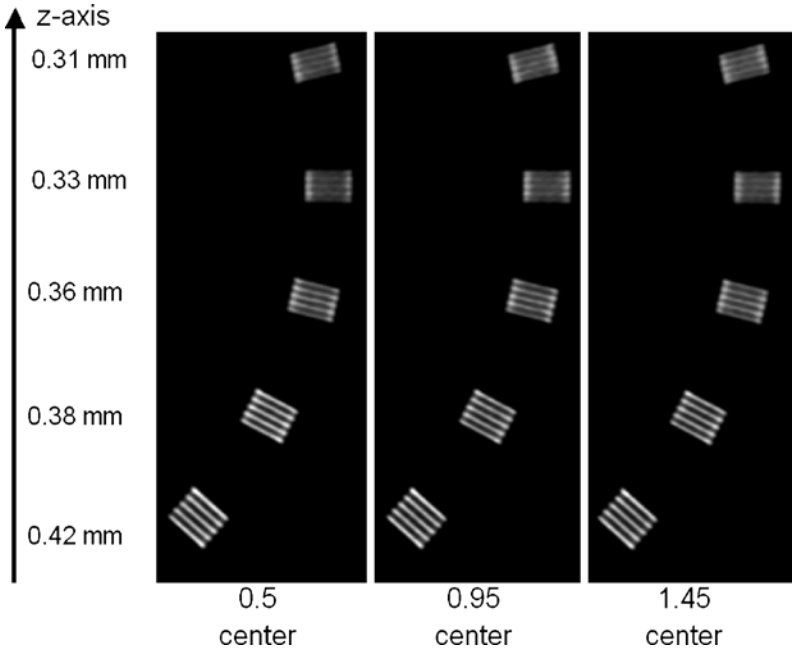

Fig. 1.12. Demonstration of *z*-axis resolution for a MDCT system using the *z*-flying focal spot technique. MPRs of a *z*-resolution phantom (high-resolution insert of the CATPHAN, the Phantom Laboratories, Salem, NY, turned by 90°) in the isocenter of the scanner as a function of the pitch. Scan data have been acquired with 32×0.6-mm collimation in a 64-slice acquisition mode using the *z*-flying focal spot and reconstructed with the narrowest slice width (nominal 0.6 mm) and a sharp body kernel. Independent of the pitch, all bar patterns up to 16 lp/cm can be visualized. The bar patterns with 15 lp/cm are exactly perpendicular to the *z*-axis, corresponding to 0.33-mm longitudinal resolution

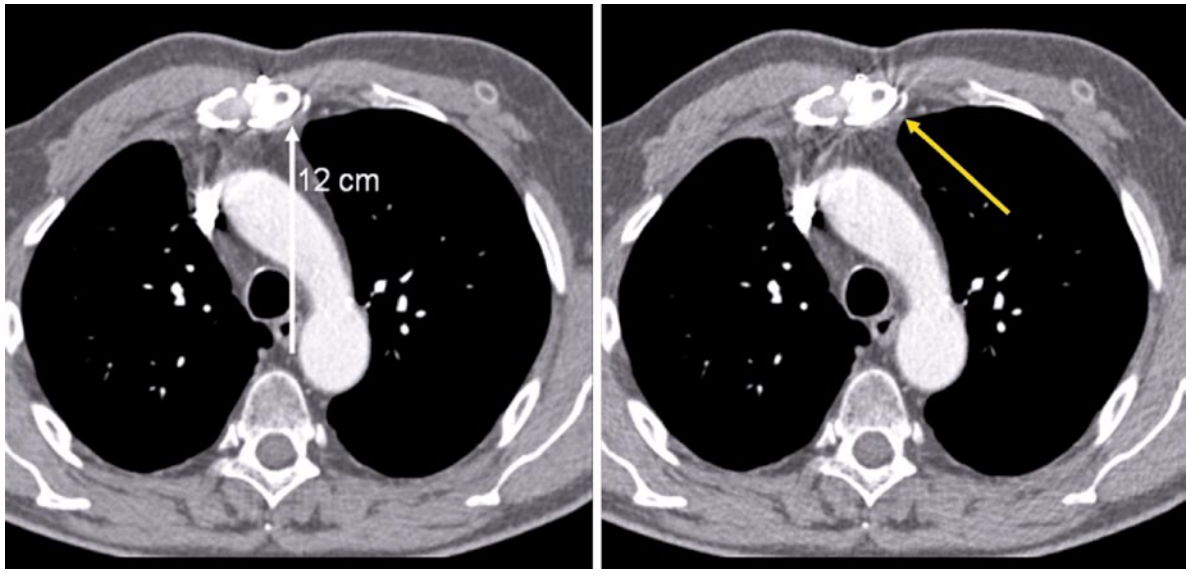

Fig. 1.13. Reduction of spiral artifacts with the *z*-flying focal spot technique. *Left*: Thorax scan with 32×0.6-mm collimation in a 64-slice acquisition mode with *z*-flying focal spot at pitch 1.5. *Right*: Same scan, using only one focus position of the *z*-flying focal spot for image reconstruction. This corresponds reasonably well to evaluating 32-slice spiral data acquired without *z*-flying focal spot. Due to the improved longitudinal sampling with *z*-flying focal spot (*left*), spiral interpolation artifacts (windmill structures at high contrast objects) are suppressed without degradation of *z*-axis resolution

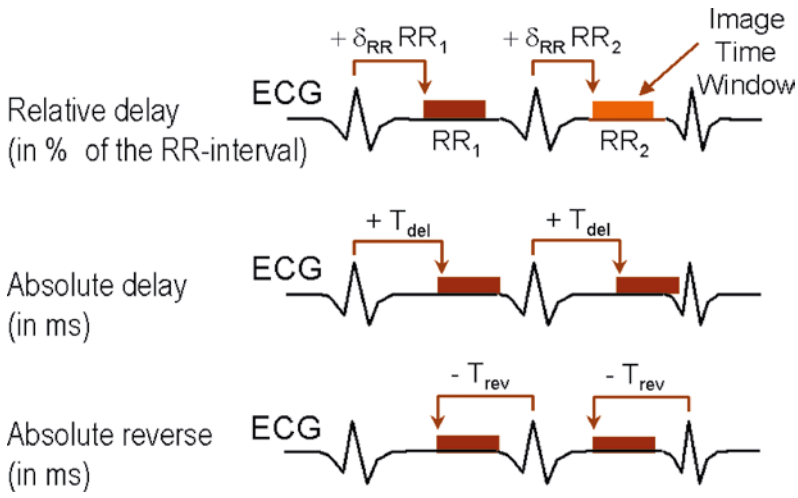

Fig. 1.14. Schematic illustration of absolute and relative phase setting for ECG-controlled CT examinations of the cardio-thoracic anatomy

SORGE 2001), which provide a temporal resolution up to half the gantry rotation time per image in a sufficiently centered region of interest. The 16-slice and 64-slice CT systems offer gantry rotation times as short as 0.4 s, 0.37 s or even 0.33 s. In this case, temporal resolution can be as good as 200 ms, 185 ms or 165 ms.

With retrospective ECG gating, the heart volume is covered continuously by a spiral scan. The patient's ECG signal is recorded simultaneously to data acquisition to allow for a retrospective selection of the data segments used for image reconstruction. Only scan data acquired in a pre-defined cardiac phase, usually the diastolic phase, are used for image reconstruction (KACHELRIESS et al. 2000; OHNESORGE et al. 2000; TAGUCHI et al. 2000; FLOHR and OHNESORGE 2001). The data segments contributing to an image start with a user-defined offset relative to the onset of the R-waves, similar to ECG-triggered axial scanning; see Fig. 1.15.

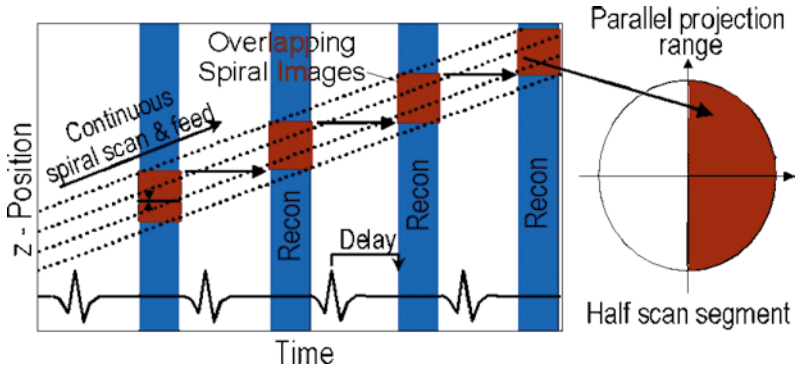

Fig. 1.15. Principle of retrospectively ECG-gated spiral scanning with single-segment reconstruction. The patient's ECG signal is indicated as a function of time on the *horizontal axis*, and the position of the detector slices relative to the patient is shown on the *vertical axis* (in this example for a four-slice CT system). The table moves continuously, and continuous spiral scan data of the heart volume are acquired. Only scan data acquired in a pre-defined cardiac phase, usually the diastolic phase, are used for image reconstruction (indicated as *red boxes*). The spiral interpolation is illustrated for some representative projection angles

Image reconstruction generally consists of two parts: multi-detector row spiral interpolation to compensate for the continuous table movement and to obtain scan data at the desired image *z*-position, followed by a partial scan reconstruction of the axial data segments (Fig. 1.15).

1.3.3.2 ECG-Gated Single-Segment and Multi-Segment Reconstruction

In a single-segment reconstruction, consecutive multi-slice spiral data from the same heart period are used to generate the single-slice partial scan data segment for an image; see Fig. 1.15. At low heart rates, a single-segment reconstruction yields the best compromise between sufficient temporal resolution on the one hand and adequate volume coverage with thin slices on the other.

The temporal resolution of an image can be improved up to $t_{rot}/(2N)$ by using scan data of N subsequent heart cycles for image formation in a so-called multi-segment reconstruction (Kachelriess et al. 2000; Taguchi et al. 2000; Cesmeli et al. 2001; Flohr and Ohnesorge 2001). t_{rot} is the gantry rotation time of the CT scanner. With increased N better temporal resolution is achieved, but at the expense of slower volume coverage: every *z*-position of the heart has to be seen by a detector slice at every time during the N heart cycles. As a consequence, the larger the N and the lower the patient's heart rate are, the more the spiral pitch has to be reduced. With this technique, the patient's heart rate and the gantry rotation time of the scanner have to be properly de-synchronized to allow for improved temporal resolution. Depending on the relationship between the rotation time and the patient heart rate, the temporal resolution is generally not constant, but varies between one half and $1/(2N)$ times the gantry rotation time in a N-segment reconstruction. There are "sweet spots," heart rates with optimum temporal resolution and heart rates where temporal resolution cannot be improved beyond half the gantry rotation time. Multi-segment approaches rely on a complete periodicity of the heart motion, and they encounter their limitations for patients with arrhythmia or patients with changing heart rates during examination. They may improve image quality in selected cases, but the reliability of obtaining good quality images with N-segment reconstruction goes down with increasing N. In general, clinical practice suggests the use of one segment at lower heart rates and $N \geq 2$ segments at higher heart rates (Flohr and Ohnesorge 2001; Flohr et al. 2003b). Image reconstruction during different heart phases is feasible by shifting the start points of the data segments used for image reconstruction relative to the R-waves. For a given start position, a stack of images at different *z*-positions covering a small sub-volume of the heart can be reconstructed due to the multi-slice data acquisition (Ohnesorge et al. 2000; Flohr and Ohnesorge 2001).

Prospective ECG-triggering combined with "step and shoot" acquisition of axial slices has the benefit of smaller patient dose than ECG-gated spiral scanning, since scan data are acquired in the previously selected heart phases only. It does, however, not provide continuous volume coverage with overlapping slices, and mis-registration of anatomical details cannot be avoided. Furthermore, reconstruction of images in different phases of the cardiac cycle for functional evaluation is not possible. Since ECG-triggered axial scanning depends on a reliable prediction of the patient's next RR interval by using the mean of the preceding RR intervals, the method encounters its limitations for patients with severe arrhythmia. To maintain the benefits of ECG-gated spiral CT, but reduce patient dose, ECG-controlled dose modulation has been developed (Jakobs et al. 2002). During the spiral scan, the output of the X-ray tube is modulated according to the patient's ECG. It is kept at its nominal value during a user-defined phase of the cardiac cycle, in general the mid- to end-diastolic phase. During the rest of the cardiac cycle, the tube output is typically reduced to 20% of its nominal values, although not switched off entirely to allow for image reconstruction throughout the entire cardiac cycle. Depending on the heart rate, dose reduction of 30–50% has been demonstrated in clinical studies (Jakobs et al. 2002).

The major improvements of 4-slice to 64-slice scanners include improved temporal resolution due to shorter gantry rotation times, better spatial resolution owing to sub-millimeter collimation and considerably reduced examination times (Flohr and Ohnesorge 2001; Flohr et al. 2003b); see Fig. 1.16.

1.3.4 Dual-Energy Computed Tomography

One of the limitations of CT is that tissues of different chemical composition but the same X-ray attenuation have the same Hounsfield values. This makes the differentiation and classification of tissue types challenging. Classical examples are the differentiation between calcified plaques and iodinated blood or hyper-dense and contrast-enhanced lesions.

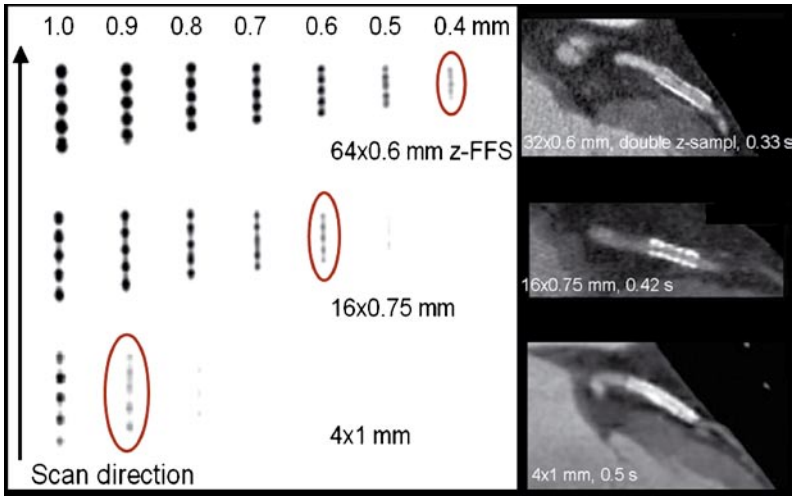

Fig. 1.16. Progress in longitudinal resolution for ECG-gated cardiac scanning from 4-slice CT to 64-slice CT. The four-slice CT scanner with 4×1-mm collimation (*bottom*) can resolve 0.9-1.0 mm objects. With 16×0.75-mm collimation, 0.6-mm objects can be delineated (*center*). The 64-slice CT scanner with 64×0.6 mm collimation and double *z*-sampling can routinely resolve 0.4-mm objects (*top*). The corresponding patient examples depict similar clinical situations (a stent in the proximal LAD). With the 64-slice system, an in-stent re-stenosis (*arrow*) can be evaluated. Four-slice case courtesy of Hopital de Coracao, Sao Paulo, Brazil; 16-slice case courtesy of Dr. A. Küttner, Tübingen University, Germany, and 64-slice case courtesy of Dr. C. M. Wong, Hong Kong, China

Besides the issue of differentiation and classification, the ambiguity of CT numbers hampers the reliability of quantitative measurements. Even for the seemingly straightforward quantification of iodine concentration, the accuracy of measured values is limited by the presence of other tissue types. For example, when determining the amount of iodine enhancement of a soft tissue lesion with use of a region of interest in that lesion measurement, the measured mean CT number will reflect not only the enhancement due to iodine, but also the underlying tissue. To overcome this limitation, additional information is required. By looking at attenuation of a material at two different energies, materials such as bone and iodine can be differentiated (Fig. 1.17).

First investigations of dual-energy methods for CT were made already in the 1970s (Macovski et al. 1976; Alvarez and Macovski 1976), but never made it into clinical routine, mainly because data for the different tube voltages had to be acquired at two different points in time. In the 1980s, it was possible to acquire dual-en-

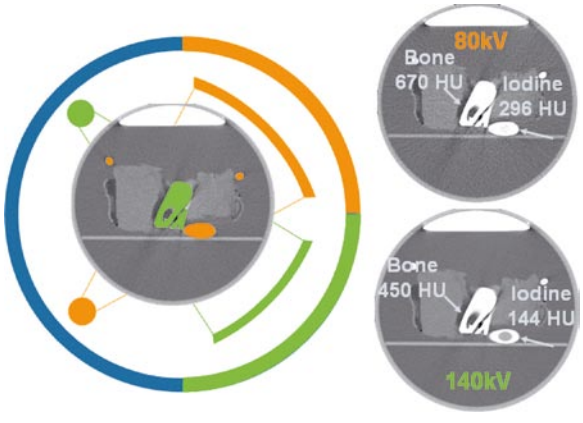

Fig. 1.17. Dual-energy principle: Using the two tubes and detectors in the Siemens SOMATOM Definition, the two tubes can be operated at different energies (80 kV and 140 kV) emmiting different X-ray spectra. In a phantom with structures with similar attenuation at one energy, such as in this example of a phantom with bone (*green*) and tubes filled with iodine (*orange*), this additional information can be used to charactize and differentiate the two materials due to their different HU values at different energies

ergy data nearly simultaneously using a modified commercial CT system (Kalender et al. 1987). During the rotation of the tube-detector pair, the tube voltage was switched quickly for each detector reading between the high and low settings so that two sets of raw data (projections) were acquired nearly simultaneously at two different tube voltages. The only application at that time was bone densitometry measurement; however, this application alone did not justify the additional costs, and dual-energy capabilities were not implemented in subsequent CT scanner generations.

With the introduction of dual-source CT, a new approach for dual-energy CT became clinically feasible. The design of this scanner allows adjusting not only the tube voltage, but also the tube current for both tube/detector pairs and allows simultaneous data acquisition. Images from both tube-detector pairs are reconstructed separately, and image-based post processing then is used to extract the dual-energy information.

Besides this approach, other acquisition methods for image-based dual-energy CT using single-source systems have been proposed. Approaches with two subsequent spiral acquisitions or two subsequent sequential scans have been reported. For static anatomical structures without any contrast enhancement dynamics, this acquisition technique appears feasible. However, for most patient scans, this prerequisite is not fulfilled. Motion, pulsation or change in contrast agent concentration between both acquisitions would lead to registration artifacts and false dual-energy information. Closer detail on the technical background and clinical applications of dual-energy CT can be found in Chaps. 5 and 36, respectively.

1.4 Future Developments

The trend towards a larger number of slices will not be driven by the need to increase scan speed in spiral acquisition modes, but rather by new clinical applications that potentially become possible with these detector and system designs. Dynamic volume imaging becomes feasible, opening up a whole spectrum of new applications, such as functional or volume perfusion studies. Recently, both Toshiba and Siemens introduced systems targeting these applications, again pursuing different technological paths to reach the same goal. Toshiba introduced a 320-slice scanner that allows covering whole organs during one rotation. It is based on the prototype scanner with 256×0.5-mm detector elements (Mori et al. 2004, 2006). Siemens introduced a 128-slice scanner with a dynamic spiral shuttle mode that also allows acquiring 4D data of large volumes. Figure 1.18 shows an example of a perfusion scan of the complete brain acquired with that technology.

Prototype systems exist that use CsI-aSi flat-panel detector technology, originally used for conventional catheter angiography, which is limited in low contrast resolution and scan speed. Short gantry rotation times <0.5 s, which are a prerequisite for successful examination of moving organs such as the heart, are beyond the scope of such systems. Spatial resolution is excellent, though, due to the small detector pixel size (Gupta et al. 2006). In pre-clinical installations, potential clinical applications of flat-panel volume CT systems are currently being evaluated (Knollmann et al. 2003; Gupta et al. 2003). The application spectrum ranges from ultra-high resolution bone imaging to dynamic CT angiographic studies and functional examinations.

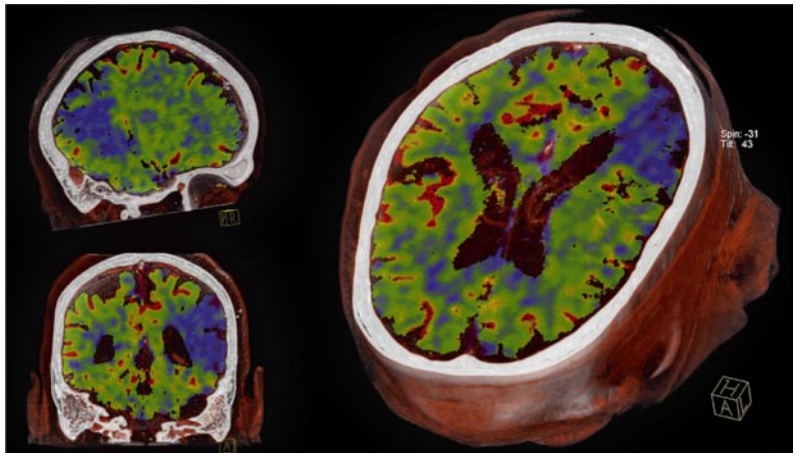

Fig. 1.18. Whole brain perfusion study on a Siemens SOMATOM Definition AS+: Using a detector configuration of 128×0.6 mm and a detector coverage of 38.4 mm, whole brain perfusion studies can be carried out by using a special spiral shuttle mode that uses a sinosoidal motion of the patient table to cover the whole brain for a period of 30 s

The combination of area detectors that provide sufficient image quality with fast gantry rotation speeds will be a promising technical concept for medical CT systems. C-arm systems already offering 3D CT capabilities are commercially available and will be discussed in Chap. 3. Compared to dedicated CT systems, which increasingly also offer support for image-guided interventions (Fig. 1.19), these scanners still offer limited image quality, but can be useful for intra-interventional imaging.

Nevertheless, it must be always kept in mind that a potential increase in spatial resolution to the level of flat-panel CT will be associated with increased dose demands, and the clinical benefit has to be carefully considered in the light of the applied patient dose. Therefore, another continued trend is saving patient dose for all kinds of clinical applications. Examples that demonstrate these efforts by the manufacturers are the introduction of dynamic collimators that eliminate the increasing problem of over-radiation in spiral scans, which was increasing with increasing detector width (Fig. 1.20), or the optimization of acquisition modes in cardiac CT, an application especially in the focus of dose discussion in the past years (Fig. 1.21).

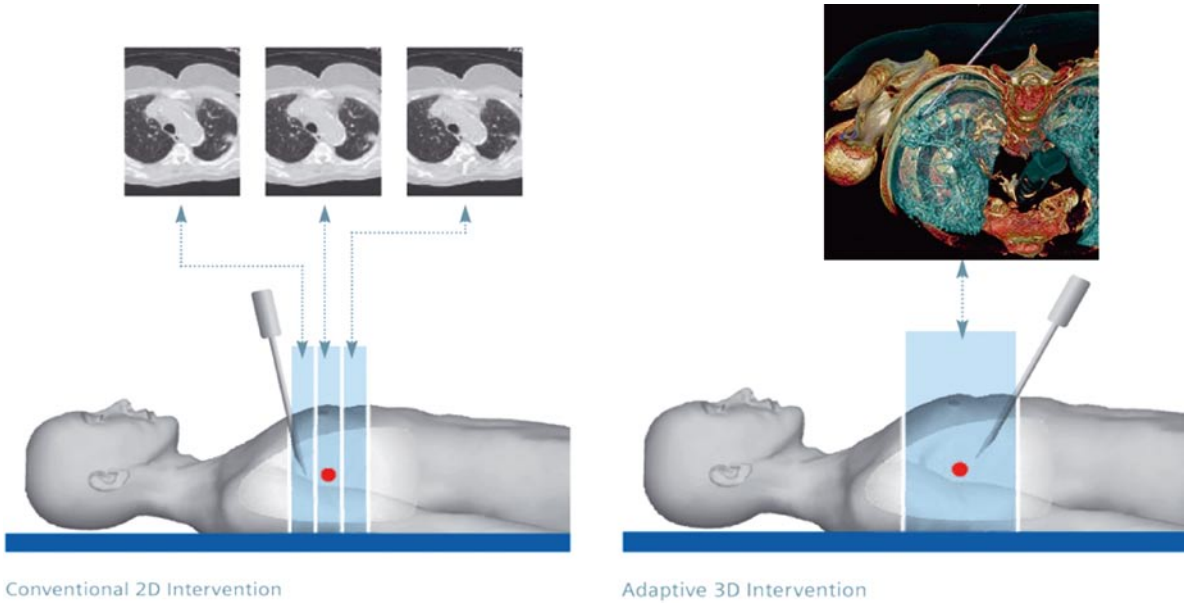

Fig. 1.19. Wider and wider detectors can also be used for interventional applications. Previously interventional CT was a 2D application due to the still limited detector coverage of up to 64 slice detectors (*left*). New visualization methods and scan modes allow real-time 3D interventions with the new generation of 128-slice scanners (*right*)

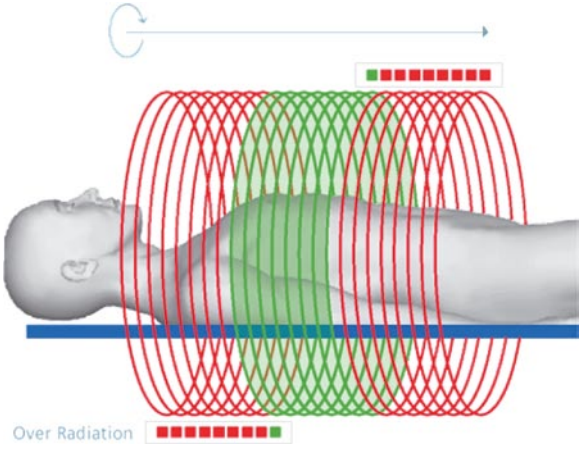

Fig. 1.20. Since the introduction of multislice detectors, it is a known issue that at the start and the end of each spiral scan, a region is irradiated for which no images can be reconstructed (*red*). That portion depends on the width of the detector and becomes more severe the wider the detector becomes and the shorter the scan region is. That problem can be overcome, but introducing a tube side collimator that continuously opens at the start of the scan and closes at the end of the scan. The Siemens SOMATOM Definition AS+ is the first scanner offering that technology, which saves 10–25 % dose depending on the application. Typical dose savings using this technology are 10% for abdominal, 15% for thorax, 20% for head and 25% for cardiac examinations

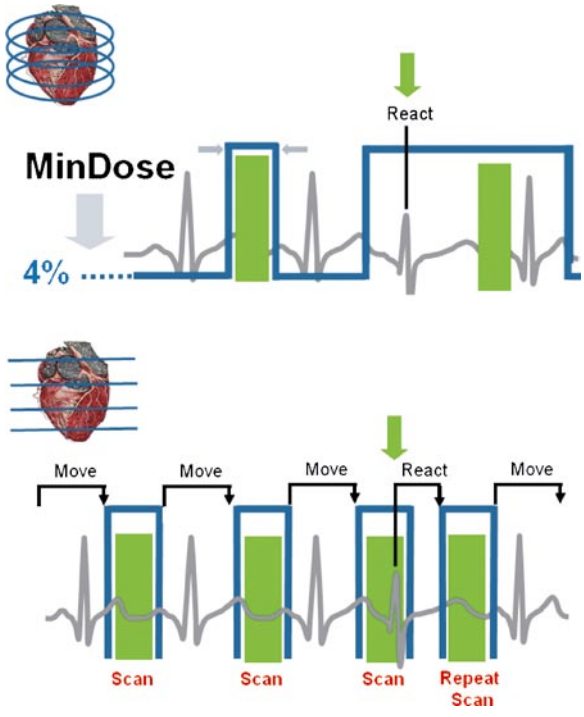

Fig. 1.21. Two competing technologies for cardiac examinations are spiral scanning using retrospective gating (*top*) and sequential scanning using prospective ECG triggering (*bottom*). Typically, retrospective gating is more robust and offers superior image quality, while prospective triggering offers additional possibilities to save dose. The recently introduced above approaches are used to make prospective triggering more robust and to save additional dose in retrospective gating. On the Siemens SOMATOM Definition platform, a functionality called "MinDose" is available that reduces the dose in heart phases that are not of interest to 4%. Additionally, it immediately reacts to irregularities in the ECG signal and raises the dose so that retrospective ECG editing becomes possible. A similar functionality was added to prospective triggering modes to make sure data are only acquired in regular heart cycles

References

Alvarez RE, Macovski A (1976) Energy-selective reconstructions in X-ray computerized tomography. Phys Med Biol 21:733-744

Cesmeli E, Edic M, Iatrou M, Pfoh A (2001) A novel reconstruction algorithm for multiphasic cardiac imaging using multislice CT. Proc SPIE Int Symp Med Imag 4320:645-654

Crawford CR, King KF (1990) Computed tomography scanning with simultaneous patient translation. Med Phys 17:967-982

Feldkamp LA, Davis LC, Kress JW (1984) Practical cone-beam algorithm. J Opt Soc Am A:612-619

Flohr T, Ohnesorge B (2001) Heart rate adaptive optimization of spatial and temporal resolution for ECG-gated multislice spiral CT of the heart. JCAT 25:907-923

Flohr T, Stierstorfer K, Bruder H, Simon J, Schaller S (2002a) New technical developments in multislice CT, part 1: Approaching isotropic resolution with sub-millimeter 16-slice scanning. Röfo Fortschr Geb Rontgenstr Neuen Bildgeb Verfahr 174:839-845

Flohr T, Bruder H, Stierstorfer K, Simon J, Schaller S, Ohnesorge B (2002b) New technical developments in multislice CT, part 2: sub-millimeter 16-slice scanning and increased gantry rotation speed for cardiac imaging. Röfo Fortschr Geb Rontgenstr Neuen Bildgeb Verfahr 174:1022-1027

Flohr T, Stierstorfer K, Bruder H, Simon J, Polacin A, Schaller S (2003a) Image reconstruction and image quality evaluation for a 16-slice CT scanner. Med Phys 30:832-845

Flohr T, Schoepf U J, Kuettner A, Halliburton S, Bruder H, Suess C, Schmidt B, Hofmann L, Yucel E K, Schaller S, Ohnesorge B (2003b) Advances in cardiac imaging with 16-section CT systems. Acad Radiol 10:386-401

Flohr T, Stierstorfer K, Raupach R, Ulzheimer S, Bruder H (2004) Performance evaluation of a 64-slice CT system with *z*-flying focal spot. Röfo Fortschr Geb Rontgenstr Neuen Bildgeb Verfahr 176:1803-1810

Flohr TG, Stierstorfer K, Ulzheimer S, Bruder H, Primak AN, McCollough CH (2005a) Image reconstruction and image quality evaluation for a 64-slice CT scanner with *z*-flying focal spot. Med Phys 32:2536-2547

Flohr TG, Schaller S, Stierstorfer K, Bruder H, Ohnesorge BM, Schoepf UJ (2005b) Multi-detector row CT systems and image reconstruction techniques. Radiology 235:756-773

Flohr T, McCollough CH, Bruder H, Petersilka M, Gruber K, Süß C et al. (2006) First performance evaluation of a dual-source CT (DSCT) system. Eur Radiol 16:256-268

Fuchs T, Krause J, Schaller S, Flohr T, Kalender WA (2000) Spiral interpolation algorithms for multislice spiral CT–Part 2: Measurement and evaluation of slice sensitivity profiles and noise at a clinical multislice system. IEEE Trans Med Imag 19:835-847

Grass M, Köhler T, Proksa R (2000) Three-dimensional cone-beam CT reconstruction for circular trajectories. Phys Med Biol 45:329-347

Gupta R, Stierstorfer K, Popescu S, Flohr T, Schaller S, Curtin HD (2003) Temporal bone imaging using a large field-of-view rotating flat-panel CT scanner. Abstract Book of the 89th Scientific Assembly and Annual Meeting of the RSNA 2003, p 375

Gupta R, Grasruck M, Süß C, Bartling SH, Schmidt B, Stierstorfer K, Popescu S, Brady T, Flohr T (2006) Ultra-high resolution flat-panel volume CT: fundamental principles, design architecture, and system characterization. Eur Radiol 16:1191

Hein I, Taguchi K, Silver M D, Kazarna M, Mori I (2003) Feldkamp-based cone-beam reconstruction for gantry-tilted helical multislice CT. Med Phys 30:3233-3242

Hsieh J (2001) Investigation of the slice sensitivity profile for step-and-shoot mode multi-slice computed tomography. Med Phys 28:491-500

Hsieh J (2003) Analytical models for multi-slice helical CT performance parameters. Med Phys 30:169-178

Hu H (1999) Multi-slice helical CT: Scan and reconstruction. Med Phys 26:5-18

Hu H, He HD, Foley WD, Fox SH (2000) Four multidetector-row helical CT: Image quality and volume coverage speed. Radiology 215: 55-62

Jakobs TF, Becker CR, Ohnesorge B, Flohr T, Suess C, Schoepf UJ, Reiser MF (2002) Multislice helical CT of the heart with retrospective ECG gating: reduction of radiation exposure by ECG-controlled tube current modulation. Eur Radiol 12:1081-1086

Kachelriess M, Ulzheimer S, Kalender W (2000) ECG-correlated image reconstruction from subsecond multi-slice spiral CT scans of the heart. Med Phys 27:1881-1902

Kalender WA, Perman WH, Vetter JR, Klotz E (1986) Evaluation of a prototype dual-energy computed tomographic apparatus. I. Phantom studies. Med Phys13:334-339

Kalender WA, Klotz E, Suess C (1987) Vertebral bone mineral analysis: an integrated approach with CT. Radiology 164:419-423.

Kalender W, Seissler W, Klotz E, Vock P (1990) Spiral volumetric CT with single-breath-hold technique, continuous transport and continuous scanner rotation. Radiology 176:181-183

Kalender W (1995) Thin-section three-dimensional spiral CT: is isotropic imaging possible? Radiology 197:578-580

Klingenbeck-Regn K, Schaller S, Flohr T, Ohnesorge B, Kopp AF, Baum U (1999) Subsecond multi-slice computed tomography: basics and applications. EJR 31:110-124

Knollmann F, Pfoh A (2003) Image in cardiovascular medicine. Coronary artery imaging with flat-panel computed tomography. Circulation 107:1209

Leschka S, Alkadhi H, Plass A, Desbiolles L, Grunenfelder J, Marincek B, Wildermuth S (2005) Accuracy of MSCT coronary angiography with 64-slice technology: first experience. Eur Heart J 26:1482-1487

Macovski A, Alvarez RE, Chan JL, Stonestrom JP, Zatz LM (1976) Energy dependent reconstruction in X-ray computerized tomography. Comput Biol Med, 6:325-336

McCollough CH, Zink FE (1999) Performance evaluation of a multi-slice CT System. Med Phys 26:2223-2230

Mori I (1986) Computerized tomographic apparatus utilizing a radiation source. US Patent 4,630,202

Mori S, Endo M, Tsunoo T, Kandatsu S, Tanada S, Aradate H et al. (2004) Physical performance evaluation of a 256-slice CT-scanner for four-dimensional imaging. Med Phys 31:1348-1356

Mori S, Endo M, Obata T, Tsunoo T, Susumu K, Tanada S (2006) Properties of the prototype 256-row (cone beam) CT scanner. Eur Radiol 16:2100-2108

Nieman K, Oudkerk M, Rensing B, van Oijen P, Munne A, van Geuns R, de Feyter P (2001) Coronary angiography with multi-slice computed tomography. Lancet 357:599-603

Nieman K, Cademartiri F, Lemos PA, Raaijmakers R, Pattynama PMT, de Feyter PJ (2002) Reliable noninvasive coronary angiography with fast submillimeter multislice spiral computed tomography. Circulation 106:2051-2054.

Nishimura H, Miyazaki O (1988) CT system for spirally scanning subject on a movable bed synchronized to X-ray tube revolution. US Patent 4,789,929

Ohnesorge B, Flohr T, Becker C, Kopp A, Schoepf U, Baum U, Knez A, Klingenbeck-Regn K, Reiser M (2000) Cardiac imaging by means of electrocardiographically gated multisection spiral CT–Initial experience. Radiology 217:564-571

Raff GL, Gallagher MJ, O'Neill WW, Goldstein JA (2005) Diagnostic accuracy of non-invasive coronary angiography using 64-slice spiral computed tomography. JACC 46:552-557

Ropers D, Baum U, Pohle K, et al. (2003) Detection of coronary artery stenoses with thin-slice multi-detector row spiral computed tomography and multiplanar reconstruction. Circulation 107:664-666

Rubin GD, Dake MD, Semba CP (1995) Current status of three-dimensional spiral CT scanning for imaging the vasculature. Radiol Clin North Am 33:51-70 (Review)

Schaller S, Flohr T, Klingenbeck K, Krause J, Fuchs T, Kalender WA (2000) Spiral interpolation algorithm for multi-slice spiral CT–Part I: Theory. IEEE Trans Med Imag 19:822-834

Schaller S, Stierstorfer K, Bruder H, Kachelrieß M, Flohr T (2001a) Novel approximate approach for high-quality image reconstruction in helical cone beam CT at arbitrary pitch. Proc SPIE Int Symp Med Imag 4322:113-127

Schaller S, Niethammer MU, Chen X, Klotz E, Wildberger JE, Flohr T (2001b) Comparison of signal-to-noise and dose values at different tube voltages for protocol optimization in pediatric CT. Abstract Book of the 87th Scientific Assembly and Annual Meeting of the RSNA 2001, p 366

Schardt P, Deuringer J, Freudenberger J, Hell E, Knuepfer W, Mattern D, Schild M (2004) New X-ray tube performance in computed tomography by introducing the rotating envelope tube technology. Med Phys 31:2699-2706